

MCMC-Correction of Score-Based Diffusion Models for Model Composition

Anders Sjöberg^{* 1 2}, Jakob Lindqvist^{* 2}, Magnus Önnheim¹, Mats Jirstrand¹, Lennart Svensson²

1. Fraunhofer-Chalmers Centre, Gothenburg, SE-412 88, Sweden.
2. Department of Electrical Engineering, Chalmers University of Technology, Gothenburg, SE-412 96, Sweden.

* Equal contribution

Abstract

Diffusion models can be parameterised in terms of either a score or an energy function. An energy parameterisation is appealing since it enables an extended sampling procedure with a Metropolis–Hastings (MH) correction step, based on the change in total energy in the proposed samples. Improved sampling is important for model compositions, where off-the-shelf models are combined with each other, in order to sample from new distributions. For model composition, score-based diffusions have the advantages that they are popular and that many pre-trained models are readily available. However, this parameterisation does not, in general, define an energy, and the MH acceptance probability is therefore unavailable, and generally ill-defined. We propose keeping the score parameterisation and computing an acceptance probability inspired by energy-based models through line integration of the score function. This allows us to reuse existing diffusion models and still combine the reverse process with various Markov-Chain Monte Carlo (MCMC) methods. We evaluate our method using numerical experiments and find that score-parameterised versions of the MCMC samplers can achieve similar improvements to the corresponding energy parameterisation.

Keywords—Diffusion models, Energy-based models, Model composition, Line integration

1 Introduction

Significant advancements have been achieved in generative modelling across various domains in recent years [2, 3, 13]. These models have become potent priors for a wide range of applications, including code generation [19], text-to-image generation [28], question-answering [3], and many others [9, 37]. Among the generative models, diffusion models [13, 31, 33] have arguably emerged as the most powerful class. Diffusion models learn to denoise corrupted inputs in small, gradual steps

and are capable of generating samples from complex distributions. They have been successful in many domains, such as generating highly realistic images [6], modelling temporal point processes [21] and even generating neural network parameters [36].

Diffusion models also offer the capability of composed sampling, which combines pre-trained models to generate samples from a new distribution. This approach, known as model composition, has a rich history [12, 16, 20, 22]. For diffusion models, the most common form of composition is classifier-guided sampling, where the reverse process is augmented by a separate classifier model [6, 14, 31], but other compositions have also been explored [7]. The ability to compose new models without having to re-learn the individual components is especially appealing for diffusion models since their ever-increasing size and data hunger make them exceedingly costly to train [1]. Therefore, it is valuable to develop sampling methods that work for pre-trained diffusion models.

The foundation of composed sampling for diffusion models is score-based, where we interpret diffusion models as predictors of the score function for the marginal distribution at each diffusion step [34]. From this perspective, MCMC methods, such as the Langevin algorithm (LA) [27] or Hamiltonian Monte Carlo (HMC) sampling [8], emerge as viable options to incorporate. Augmenting the standard reverse process with additional MCMC sampling has been shown to improve composed sampling for diffusion models [7]. However, we are restricted to unadjusted variants of these samplers, namely Unadjusted LA (U-LA) and Unadjusted HMC (U-HMC), which only require utilization of the score. This limitation means we cannot incorporate a Metropolis-Hastings (MH) correction step [10, 23], which requires evaluating the unnormalized density.

An intriguing alternative to directly modeling the score function is to model the marginal distribution with an energy function, from which the score can be obtained through explicit differentiation [29, 33]. This parameterization connects diffusion models and energy-based models (EBMs) [18] and offers several desirable properties. With an energy parameterization, we can evaluate the unnormalized density and guarantee a proper score function. This, in turn, enables an MH correction step when employing a MCMC-method, where the MH acceptance probability is computed from the energy function. Adding such a correction step has been shown to improve sampling performance in composed models [7]. Nevertheless, the score parameterization remains far more popular, as it avoids the direct computation of the gradient of the log density.

In this study, we build on the work in [7] and introduce a novel approach to obtain a form of MH-like correction directly from pre-trained diffusion models without relying on an energy-based parameterisation. Specifically, we use a connection between the score and the energy to estimate the MH acceptance probability by approximating a line integral along the vector field generated by the score of the composed diffusion models. This enables an improved sampling procedure for various pre-trained score-parameterised diffusion models.

We approximate the line integral using the trapezoidal rule and validate the effectiveness of our MH-like correction by sampling from different composed distributions and comparing it with an energy-based parameterisation. We find that our approximate method quantitatively results in improvements comparable to the energy parameterisation, without having to estimate the energy directly.

2 Background

2.1 Diffusion Models

We consider Gaussian diffusion models initially proposed by [31] and further improved by [33] and [13]. Starting with a sample from the data distribution $x_0 \sim q(\cdot)$, we construct a Markov

chain of latent variables x_1, \dots, x_T by iteratively introducing Gaussian noise to the sample

$$q(x_t | x_{t-1}) = \mathcal{N}\left(x_t; \sqrt{1 - \beta_t}x_{t-1}, \beta_t I\right), \quad (1)$$

where $\beta_t \in [0, 1)$, $\forall t = 1, \dots, T$ are known. For large enough T we have $q(x_T) \approx \mathcal{N}(x_T; 0, I)$.

A diffusion model learns to gradually denoise samples by modelling the distribution of the previous sample in the chain $p_\theta(x_{t-1} | x_t)$, $t = 1, \dots, T$. Approximate samples from the data distribution $q(x_0)$ are obtained by starting from $x_T \sim \mathcal{N}(0, 1)$ and sequentially sampling less noisy versions of the sample until the noise is removed. This is called the *reverse process*.

The reverse distribution is typically modelled as

$$p_\theta(x_{t-1} | x_t) = \mathcal{N}\left(x_{t-1}; \mu_\theta(x_t, t), \Sigma_\theta(x_t, t)\right), \quad (2)$$

since the posterior, reverse, distribution $q(x_{t-1} | x_t)$ can be effectively approximated by a Gaussian distribution, when the magnitude β_t of the noise added at each step is sufficiently small. The mean of this distribution is parameterised as

$$\mu_\theta(x_t, t) = \frac{1}{\sqrt{\alpha_t}} \left(x_t - \frac{\beta_t}{\sqrt{1 - \bar{\alpha}_t}} \epsilon_\theta(x_t, t) \right), \quad (3)$$

where the parameters α_t and $\bar{\alpha}_t$ are functions of $\{\beta_t\}_{t=1}^T$ [13]. The noise prediction model $\epsilon_\theta(x_t, t)$ is typically parameterised as a neural network and learned from data. A common choice is to set $\Sigma_\theta(x_t, t) = \beta_t I$, which we assume throughout this paper unless stated otherwise.

A useful property that simplifies the training is that the conditional diffusion probability $q(x_t | x_0)$ can be computed in closed form

$$q(x_t | x_0) = \mathcal{N}\left(x_t; \sqrt{1 - \sigma_t^2}x_0, \sigma_t^2 I\right), \quad (4)$$

for any t , where σ_t is a function of $\{\beta_t\}_{t=1}^T$. We refer to [13] for a detailed derivation.

2.2 Energy-based models

Energy based-models (EBM) represent probability distributions with a scalar, non-negative energy function E_θ , by assigning low energy to regions of the input space where the probability is high and high energy to regions where the distribution has little or no support:

$$p_\theta(x_t, t) = \frac{1}{Z_\theta(t)} \exp(-E_\theta(x_t, t)), \quad Z_\theta(t) = \int \exp(-E_\theta(x_t, t)) dx_t. \quad (5)$$

Here, we let E_θ depend on the time step t to make the connection to diffusion models more apparent. This can be interpreted as a sequence of energy functions, one for each diffusion step t . The normalisation constant Z_θ is typically intractable, prohibiting computing a normalised density. However, Z_θ does not depend on the input x_t , making the so-called *score function* easy to compute for an EBM:

$$\nabla_x \log p_\theta(x_t, t) = -\nabla_x E_\theta(x_t, t), \quad (6)$$

even though the gradient of the energy function can be costly to compute in practice.

2.3 Energy and score parameterised diffusion models

The foundation of this paper is that the diffusion noise prediction model $\epsilon_\theta(x_t, t)$ can be interpreted as estimating a quantity proportional to the score function of the marginal distribution $q(\cdot)$ at diffusion step t [34]

$$\epsilon_\theta(x_t, t) \approx -\sigma_t \nabla_x \log q(x_t). \quad (7)$$

This property provides a connection between diffusion and energy-based models. We can now model

$$\frac{1}{\sigma_t} \epsilon_\theta(x_t, t) = -\nabla_x \log p_\theta(x_t, t) = \nabla_x E_\theta(x_t, t). \quad (8)$$

That is, the marginal distribution $q(x_t)$ can be approximated using either an energy function E_θ or a noise prediction model ϵ_θ . This results in two methods for parameterising the model of $q(x_t)$: the *energy parameterisation*, using E_θ , and the *score parameterisation*, using ϵ_θ .

Both parameterisations have their advantages and disadvantages. The energy parameterisation can evaluate the density $p_\theta(x_t, t)$ up to a normalisation $Z_\theta(t)$, which enables various MCMC methods. Furthermore, by making the score equal to the gradient of an actual scalar function, we ensure a proper score, i.e., a conservative vector field. On the other hand, to evaluate the score function, E_θ must be explicitly differentiated, which can be costly.

The score parameterisation is more flexible since it predicts an arbitrary vector field. There is limited empirical evidence that this results in better sampling performance with the diffusion process [7], although it has been suggested that this performance difference is mainly due to model architecture [29]. Regardless, the fact that the score parameterisation directly estimates the score function makes it more efficient for sampling with the reverse process, and the score parameterisation is, by far, the more popular variant.

This paper aims to develop methods that improve the standard sampling with the reverse process while still retaining the ability to compose pre-trained diffusion models. Since the score parameterised diffusion models are more prevalent, developing similarly corrected MCMC samplers for the score parameterisation is desirable.

3 MCMC sampling for diffusion models

MCMC sampling is a promising strategy for improving diffusion model sampling since it can be used in combination with the reverse process. Just like the reverse process, there are MCMC methods which base their kernels on the score function, such as the Unadjusted Langevin Algorithm (U-LA) and the Unadjusted Hamiltonian Monte Carlo (U-HMC) [8, 24, 27]. For example, with U-LA we use the kernel

$$k_t(x^{\tau+1} | x^\tau) = \mathcal{N}(x^{\tau+1}; x^\tau + \delta_t \nabla_x \log p_\theta(x^\tau, t), 2\delta_t I), \quad (9)$$

at diffusion step t , where $x^0 = x_t$, δ_t is the step size, and the chain is iterated for L steps.

These methods are called unadjusted, since as L grows, these samplers will converge to the target distribution, but only for infinitesimal step sizes δ_t . By adding, for instance, a Metropolis–Hastings (MH) correction step, we can sample with larger step sizes and still converge to the target distribution [10, 23]. With the correction, we sample a candidate $\hat{x} \sim k_t(\cdot | x^\tau)$ and accept it as the new iterate with probability

$$\alpha = \min\left(1, \frac{p_\theta(\hat{x}, t)}{p_\theta(x^\tau, t)} \frac{k_t(x^\tau | \hat{x})}{k_t(\hat{x} | x^\tau)}\right). \quad (10)$$

That is, we set the new iterate $x^{\tau+1} = \hat{x}$ with probability α , otherwise $x^{\tau+1} = x^\tau$.

The model p_θ appears in the acceptance probability as a ratio, meaning that we do not require a normalised density to compute α , since the normalisation constant depends only on the relative probability between the current and proposed sample. Furthermore, if p_θ is an EBM (see eq. (5)), the probability ratio can be expressed as

$$\frac{p_\theta(\hat{x}, t)}{p_\theta(x^\tau, t)} = \exp(E_\theta(x^\tau, t) - E_\theta(\hat{x}, t)). \quad (11)$$

This means that with an EBM we can evaluate the MH acceptance probability to construct an adjusted MCMC sampler. This is an important advantage compared to the score parameterisation, where we only have access to $\nabla_x \log p_\theta$ (see eq. (8)).

3.1 Sampling from composed models

Augmenting the reverse process with additional MCMC sampling appears to be important in diffusion model composition [7,33], which combines pre-trained score functions to sample from new marginal distributions using the reverse process. The most common form of model composition is called *guidance* [6], where the goal is to sample from a distribution conditioned on a class label y

$$q(x_0 | y) \propto q(x_0)q(y | x_0). \quad (12)$$

This is achieved by composing a score function from an unconditional diffusion model (using eq. (8)) for the marginal distribution and a classifier for the likelihood

$$\nabla_x \log p_{\theta'}(x_t | y, t) = \nabla_x \log p_\theta(x_t, t) + \lambda \nabla_x \log p_\varphi(y | x_t, t), \quad (13)$$

i.e., the classifier guides the reverse process by modifying the score function towards samples whose predicted class is y . In practice, a hyperparameter λ is introduced in order to control the strength of the guidance.

Several proposed variations exist for the guidance model. The most straightforward way is to learn a sequence of classifiers for each noise level t , which was proposed by [6], which we term *classifier-full guidance*. Another option is to use a single noise-free classifier $p(y|x_0)$ and use the score function to de-noise the input $x_0 \approx \hat{x}_\theta(x_t, t)$, this method is called *reconstruction guidance* [4, 15, 32]. Finally, there is *classifier-free guidance*, which does not use a classifier but composes a conditional and an unconditional diffusion model [14]. Note that this no longer corresponds to sampling from the posterior distribution in eq. (12).

In [7], they investigate further forms of compositions: products, mixtures, and negations. For example, they model a product distribution as

$$q^{\text{prod}}(x_0) \propto \prod_i q^i(x_0). \quad (14)$$

While this factorisation generally only holds at $t = 0$, they form a composed model

$$p_\theta^{\text{prod}}(x_t, t) \propto \prod_i p_{\theta_i}^i(x_t, t) = \exp\left(-\sum_i E_{\theta_i}^i(x_t, t)\right) \quad (15)$$

and perform MCMC sampling with this as the target distribution, resulting in increased sampling performance. Note that the composition in eq. (15) is also viable with a score parameterisation, where the composed score

$$\nabla_x \log p_\theta^{\text{prod}}(x_t, t) \propto \nabla_x \log \prod_i p_{\theta_i}^i(x_t, t) = \sum_i \nabla_x \log p_{\theta_i}^i(x_t, t) = -\frac{1}{\sigma_t} \sum_i \epsilon_{\theta_i}^i(x_t, t) \quad (16)$$

is the sum of the component scores.

4 MCMC-correction with the score parameterisation

We propose to combine the properties of the energy parameterisation with the performance and greater availability of the score parameterization. Instead of using an energy parameterization and computing the score by differentiation, we take the reversed approach, use a score parameterization and compute the change in (pseudo-)energy by integrating the score.

4.1 Recovering pseudo-energy difference from the score

This section describes how MCMC acceptance probabilities can be approximated given a score function. The MH acceptance probability in eq. (10) is based on the relative probability of the new candidate \hat{x} and the current sample x^τ . The transition probabilities given by the kernel $k_t(\cdot | \cdot)$ are assumed to be simple to compute and we focus on the quotient $p_\theta(\hat{x})/p_\theta(x^\tau)$. To compute the MH acceptance probability α , we only need to evaluate the unnormalised target distribution. For an EBM, this requirement can be further relaxed since α can be expressed in terms of the difference in energy at \hat{x} and x^τ , see eq. (11). That is, we do not need to compute the absolute value of the energy, only the difference.

To express the acceptance probability in terms of the score function, we write the difference in energy as a line integral on a curve \mathcal{C}

$$E_\theta(x^\tau, t) - E_\theta(\hat{x}, t) = - \int_{\mathcal{C}} \nabla_r E_\theta(r, t) \cdot dr = - \int_0^1 \nabla_r E_\theta(r(s), t) \cdot r'(s) ds, \quad (17)$$

where $r(s)$ is a parameterisation of \mathcal{C} such that $r(0) = x^\tau$ and $r(1) = \hat{x}$. The curve parameterisation is arbitrary (under mild conditions) since E_θ is a scalar field.

For a score-parametrised diffusion model, we propose to use the relation between the score function and ϵ_θ from eq. (8) to calculate an MH-like ratio as

$$\alpha = \min \left(1, \exp [f(\hat{x}, x^\tau, t)] \frac{k_t(x^\tau | \hat{x})}{k_t(\hat{x} | x^\tau)} \right) \quad (18)$$

where

$$f(\hat{x}, x^\tau, t) = - \int_0^1 \frac{\epsilon_\theta(r(s), t)}{\sigma_t} \cdot r'(s) ds, \quad (19)$$

representing our constructed pseudo-energy difference. Note that if the score $-\frac{\epsilon_\theta(x, t)}{\sigma_t} = \nabla_x F(x, t)$ for some function F , eq. (19) can be interpreted as recovering an (unknown) energy function, and in this case eq. (18) agrees with eq. (10). In general, however, no such function F exists, and the expression eq. (19) depends on the path r that is integrated over. Nevertheless, we propose to use eq. (18) to directly model an MH-like acceptance probability, to be used in an MCMC sampling scheme. An overview of our proposed sampling method is given in algorithm 1.

Since eq. (19) in general depends on the path r between x^τ and \hat{x} , we propose two variants for the curve \mathcal{C} : first is the obvious option of a straight line connecting the two points and the second is a curve running through points where we have already evaluated the score function. The motivation for the latter option is to reduce the computational burden since evaluating the score is a bottleneck. Some MCMC methods (notably HMC), require the score at some additional points apart from the current sample. By choosing a curve which incorporates these points, we achieve greater numerical accuracy, essentially for free.

Specifically, we approximate the line integral with the trapezoidal rule, where the number of line segments used to approximate the curve \mathcal{C} is treated as a hyperparameter. Note that we have

Algorithm 1 MCMC reverse diffusion sampling

Require: $\epsilon_\theta(\cdot, t)$, β_t , α_t , $\bar{\alpha}_t$, T , L , δ_t , ψ (remaining hyperparameters for MCMC method)

$x_T \sim \mathcal{N}(0, I)$

for $t = T, \dots, 1$ **do** ▷ Reverse diffusion

$\epsilon \sim \mathcal{N}(0, I)$

$x_{t-1} = \frac{1}{\sqrt{\alpha_t}} \left(x_t - \frac{\beta_t}{\sqrt{1 - \bar{\alpha}_t}} \epsilon_\theta(x_t, t) \right) + \sqrt{\beta_t} \epsilon$

$x^{\tau=0} = x_{t-1}$

if $t > 1$ **then** ▷ MCMC-sampler at each $t - 1$

for $\tau = 1, \dots, L$ **do**

$x^\tau = \text{MCMC-sampler}(\epsilon_\theta, x^{\tau-1}, \tau, t - 1, \delta_{t-1}, \psi)$

end for

$x_{t-1} = x^{\tau=L}$

end if

end for

return x_0

to evaluate ϵ_θ at some internal points on \mathcal{C} , incurring an additional computational burden (except for those we can re-use in the HMC case), but we avoid differentiating the model by estimating the score function directly, using ϵ_θ . Conversely, the energy parameterisation only evaluates the energy at x^τ and \hat{x} , but has to differentiate E_θ to obtain the score.

4.2 MH-correction for composition models

Our proposed method applies to product compositions and, consequently, enables guidance. For a product distribution in eq. (15), we have a sum of energies in the exponent, which we can approximate from the score models $\epsilon_{\theta_i}^i(x_t, t)$, using the line integral in eq. (17)

$$\begin{aligned} E_\theta^{\text{prod}}(\hat{x}, t) - E_\theta^{\text{prod}}(x^\tau, t) &= \sum_i E_{\theta_i}^i(\hat{x}, t) - \sum_i E_{\theta_i}^i(x^\tau, t) = \int_0^1 \sum_i \nabla_r E_{\theta_i}^i(r(s), t) \cdot r'(s) ds \\ &= \frac{1}{\sigma_t} \int_0^1 \sum_i \epsilon_{\theta_i}^i(r(s), t) \cdot r'(s) ds. \end{aligned} \quad (20)$$

For guidance, the score is composed of two terms according to eq. (13), where the first term is an unconditional diffusion model ϵ_θ and the second term is the score of a classifier $p_\varphi(y | x_t, t)$. The energy difference for the composed guidance score can in principle, be estimated using eq. (20), but since we can evaluate $p_\varphi(y | x_t, t)$ directly, only the energy difference for ϵ_θ needs to be estimated with the line integral.

The score for a negation composition (as formulated in [7]) can be computed analogously. Mixtures, however, are less suitable for this method as they cannot be described as a pseudo-energy difference. One could argue that a similar integration idea can be employed to recover an pseudo-energy at x simply by integrating from an arbitrary fixed point x^0 to x . However, this would involve integration along a potentially lengthy curve, which has several disadvantages. Firstly, it requires a more refined mesh for the numerical integration. Secondly, as the estimated score is generally not a proper conservative field, the choice of curve will have a greater effect over long distances, making the method less robust.

5 Results

We investigate the impact of our MH-like correction step on different forms of model composition, aiming to draw samples from a composed distribution using diffusion models trained solely on the individual components’ distributions. That is, the model components are fixed, and we sample from the composed distribution, incorporating MCMC steps at each diffusion step. Our code is available at our GitHub repo¹.

In the first two experiments, we train the diffusion models ourselves with both energy and score parameterization. The experimental setups for these cases are similar: the score parameterization is defined by a noise prediction model $\epsilon_\theta(x_t, t)$. For the energy parameterization, we follow the setup in [7] and estimate the energy function as

$$E_\theta(x_t, t) = \|x_t - s_\theta(x_t, t)\|_2^2, \quad (21)$$

where s_θ is a vector-valued output of a neural network with the same dimension as x_t . The score-based ϵ_θ has an identical network architecture to s_θ . Both score and energy-parameterized models are trained with the standard diffusion loss [13], with the score function of the energy-based model obtained through explicit differentiation.

In the third and fourth experiments, we utilize larger pre-trained score-based diffusion models to test our proposed method. However, we do not have energy-based models for comparison in these cases.

We evaluate both unadjusted and MH-corrected versions of LA and HMC. We compare the sampling performance of the score and energy-parameterized models, when available, to the standard reverse process, which serves as the baseline.

For the MH-like correction, we evaluate two types of curves along which the score is integrated: *line* and *curve*. *Line* corresponds to a straight line from x^τ to \hat{x} (see eq. (19)), while *curve* corresponds to integration along a curve that incorporates the internal points of an MCMC method (in this case, the leapfrog steps of HMC). Furthermore, the number of points used for the trapezoidal rule’s mesh for the line integral per MCMC step is treated as a hyperparameter. However, since several points are evaluated regardless in the MCMC method, e.g., x^τ and \hat{x} , we let the hyperparameter describe the number of points in addition to those we get for free. These additional points are evenly distributed along the curve.

5.1 2D composition

We repeat the 2D product composition example from [7]. The experimental setup is identical to theirs unless otherwise specified. Further details are given in appendix A.1

A pair of 2D densities are composed by multiplication into a more complex distribution, as in eq. (15). We consider a Gaussian mixture with 8 modes evenly distributed along a circle and a uniform distribution that covers two modes of the Gaussian mixture. For a visual representation of the two individual distributions and their resulting product distribution together with samples from the reverse diffusion and HMC corrected samples, see fig. 1. For the baseline reverse diffusion process, we use $T = 100$ diffusion steps. The MCMC versions add an extra sampling procedure at each diffusion step t , refining the samples of the reverse process. In [7], they omit the reverse step from the sampling, and we do the same to make the comparison more similar, but it is trivial to reinstate the reverse step into the sampling process. The MCMC sampling is run for $L = 10$ at each t , where (U-)HMC uses 3 leapfrog steps per MCMC step.

¹https://github.com/FraunhoferChalmersCentre/mcmc_corr_score_diffusion

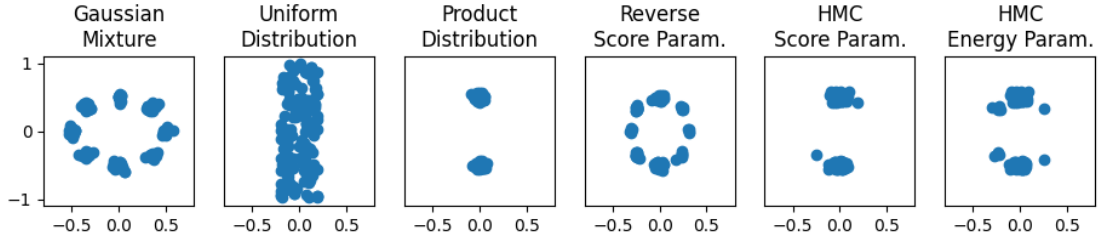


Figure 1. The two leftmost figures illustrate samples from two individual distributions: a Gaussian mixture and a uniform distribution. The third figure presents samples from the true product distribution. The fourth figure exhibits samples obtained through the reverse process utilizing score parameterization. On the right side, the last two figures display samples acquired through HMC sampling using both score and energy parameterization.

We consider three metrics to evaluate performance. The first metric is the log-likelihood (LL), where we compare the likelihood of generated samples under the true data distribution, following [7]. We may, however, sample points outside the support of the true distribution. It is unclear how this issue is handled in [7], but we address it by adding a small uniform probability to extend the support to the sampled points. Full details are provided in the appendix A. The second metric is referred to as a Gaussian mixture model (GMM). In this metric, we sample from both the true and data distributions. Then, we fit a bi-modal GMM to each set of samples and compute the Frobenius norm of the mean difference of the variances. Finally, we supplement the metrics with the Wasserstein-2 distance (W_2) to quantify a measure between the data and model distribution [35]. To achieve this, we draw samples from the data and model distributions and compute W_2 by finding the optimal assignment between the two sampled sets.

We report quantitative results for the 2D composition in table 1. The results are averaged over 10 independent trials. In each trial, we train the two diffusion models from scratch and sample 2000 points with different MCMC methods. The results demonstrate superior performance of the adjusted sampling methods compared to the unadjusted approaches. Additionally, the HMC-variants achieve better results than Langevin, while the reverse process performs worse. Score and energy parameterisations exhibit similar overall performance in LL and GMM within their respective sampling procedures. However, when paired with HMC, the score parameterisation significantly outperforms the energy parameterisation in terms of Wasserstein 2-distance. Further, we note that the performance plateaus when using as few as four points in the trapezoidal rule.

5.2 Guided diffusion for CIFAR-100

We evaluate our proposed sampling methods for guided diffusion sampling on the CIFAR-100 image dataset [17]. The sampling process is based on a score function defined in eq. (13), composed of the score functions of a marginal distribution $\nabla_x \log p_\theta(x_t, t)$ and a likelihood of the class y , $\nabla_x \log p(y | x_t, t)$, at each diffusion step $t = 1, \dots, T$.

The score of the marginal distribution $\nabla_x \log p_\theta(x_t, t)$ is estimated with an unconditional diffusion model. The score parameterised model is $\epsilon_\theta : \mathbb{R}^{D_x \times 1} \rightarrow \mathbb{R}^{D_x}$, where $D_x = 3 \cdot 32^2$, takes a noisy image and t as input and outputs a noise prediction of the same shape as x_t . It is parameterised by a neural network with a UNet architecture. We use the same architecture and training settings as [13] used for the CIFAR-10 image dataset [17]. The energy parameterised model uses the same architecture and is parameterised as in eq. (21).

For the guidance model, we use classifier-full guidance, that is, we train a classifier model

Table 1. Quantitative results for 2D composition. The mean and standard deviation for the LL, W_2 , and GMM metrics are computed for the product compositions in fig. 1, for both score and energy parameterised models. The metrics are based on 10 independent trials, wherein each trial, we re-train the diffusion model components and generate 2000 samples. For the score parameterisation, we report results for different numbers of additional points in the trapezoid rule and integration curves ("line" indicates a straight path, while "curve" means integrating along the trajectory formed by exploratory points used by HMC to propose new points).

Model	Sampler	LL \uparrow	$W_2\downarrow$	GMM \downarrow
Energy	Reverse	-8.22 ± 0.21	5.81 ± 0.19	0.02701 ± 0.00134
	U-LA	-7.52 ± 0.22	4.19 ± 0.45	0.01461 ± 0.00135
	LA	-6.50 ± 0.30	4.24 ± 0.55	0.01466 ± 0.00146
	U-HMC	-5.72 ± 0.18	4.19 ± 1.25	0.00653 ± 0.00091
	HMC	-4.09 ± 0.14	4.12 ± 1.44	0.00333 ± 0.00065
Score	Reverse	-8.15 ± 0.24	5.80 ± 0.20	0.02688 ± 0.00120
	U-LA	-7.57 ± 0.12	4.44 ± 0.63	0.01499 ± 0.00062
	LA-1-line	-6.45 ± 0.20	4.03 ± 0.52	0.01428 ± 0.00107
	LA-3-line	-6.61 ± 0.17	4.22 ± 0.46	0.01519 ± 0.00092
	LA-8-line	-6.53 ± 0.17	4.20 ± 0.51	0.01475 ± 0.00091
	U-HMC	-5.77 ± 0.12	3.39 ± 0.77	0.00690 ± 0.00071
	HMC-1-line	-4.29 ± 0.13	2.92 ± 1.02	0.00372 ± 0.00061
	HMC-3-line	-4.07 ± 0.13	2.68 ± 1.20	0.00308 ± 0.00069
	HMC-8-line	-4.07 ± 0.14	2.87 ± 0.89	0.00317 ± 0.00056
	HMC-curve	-4.07 ± 0.12	2.94 ± 0.90	0.00306 ± 0.00054

to predict the class label of an image at all diffusion steps $p_\varphi(y | x_t, t)$, where the classifier parameters φ are independent of θ . The classifier model is parameterised by a neural network with the first half of the UNet structure used for the unconditional diffusion model extended with a dense layer. To train the classifier, we use labelled pairs (x_t, y) , where y is the class and $x_t \sim q(x_t | x_0)$ is a sample from the forward diffusion process in eq. (4), conditioned on a sample x_0 from the data distribution.

The sampling is based on the standard reverse process with $T = 1000$. The MCMC samplers add $L = 2$ or 6 extra MCMC steps at each diffusion step t for (U-)HMC and (U-)LA, respectively, whereas (U-)HMC uses 3 leapfrog steps per MCMC step. All sampling methods use the same guidance scale $\lambda = 20.0$.

For this experiment, we need to use more points in the trapezoidal rule’s mesh than in the 2D experiment. Based on the insights from that experiment, for HMC we integrate only along the curve obtained from the leapfrog steps. However, we also evaluate a point in the middle of each leapfrog step to obtain a better energy estimation, resulting in three extra model evaluations per HMC step. For LA, we use seven evaluation points along the line, which means eight extra evaluations per step.

Recognising the impact of the step length on MCMC methods in general, we parameterise the step length as a function of the beta-schedule $\delta_t = a\beta_t^b$. We conducted a simple parameter search for parameters a and b , to determine suitable step length for each MCMC variant. Further details are provided in appendix A.2.

We sample 50k images with each sampling method, for both the energy and score parameterisations and compute the FID score [11] (based on the validation set) and the average accuracy² of a separate classifier model, trained only on noise-free pairs (x_0, y) from the CIFAR-100 dataset. The model architecture of the classifier is VGG-13-BN from [30]. The results are shown in table 2. From the table, we note a general trend of improvement of the baseline reverse process when additional MCMC steps are added. In particular, the MH-corrected samplers LA and HMC show significant improvement in the FID score, which is arguably the more important metric for image generation.

Comparing the score and energy parameterisations, the respective performances have largely shared characteristics. Interestingly, the basic reverse process favours the score parameterisation supporting the claim that this less restricted parameterisation better models the score function of the marginal distribution. However, the energy parameterisation sees larger improvements from the added MCMC steps. This indicates, perhaps, that the direct energy estimation provides a better correction step compared to our method of approximating the pseudo-energy difference from ϵ_θ , though it should be noted that the same difference is also observed in the unadjusted samplers U-LA and U-HMC. Despite the performance edge of the energy parameterisation, our proposed MH-corrected sampling methods can provide essentially the same improvement, without having to train an energy parameterised diffusion model.

5.3 Guided diffusion for ImageNet

We extend the evaluation of our proposed method for guided diffusion sampling on the ImageNet dataset [5]. We utilize pre-trained score models from [6], available on the OpenAI GitHub repository³.

As in the CIFAR-100 experiments, the score of the marginal distribution $\nabla_x \log p_\theta(x_t, t)$ is estimated using an unconditional diffusion model. For the ImageNet dataset, the score

²We classify an image as correctly generated if the classifier has predicted the specified class and is 50% certain or greater.

³<https://github.com/openai/guided-diffusion>

Table 2. Average accuracy and FID score for classifier-full guidance on CIFAR-100. The metrics are based on 50k generated samples for each sampling method with both energy and score parameterisations. We use the guidance scale $\lambda = 20.0$, the (U-)LA methods use $L = 6$ MCMC steps, and (U-)HMC use $L = 2$ with 3 leapfrog steps for the variants, the step length at diffusion step is $a\beta_t^b$. The accuracy is based on a separate model, which has only been trained on noise-free samples, i.e., it predicts $p(y | x_0)$. Both parameterizations benefit from the added MCMC steps, especially the MH-corrected versions. The energy parameterisation appears to perform worse in the standard reverse process but sees a larger improvement from the extra MCMC steps.

Model	Sampler	Accuracy [%]↑	FID↓
Energy	Reverse	72.6	33.4
	U-LA	87.3	24.6
	LA	80.0	12.7
	U-HMC	87.2	25.4
	HMC	84.9	12.4
Score	Reverse	74.2	31.8
	U-LA	82.9	25.9
	LA-8-line	75.2	15.5
	U-HMC	79.0	28.6
	HMC-3-curve	75.8	13.3

parameterized model, $\epsilon_\theta : \mathbb{R}^{D_x} \times 1 \rightarrow \mathbb{R}^{D_x}$, where $D_x = 3 \cdot 256^2$, is also parameterized by a neural network with a UNet architecture. Again, we use classifier-full guidance, and the classifier model is parameterised by a neural network with the structure of the corresponding encoder part of the UNet.

Given the high computational demands due to both the large models and high-dimensional input, we have chosen to focus solely on evaluating HMC (with our MH-like correction) and compare it to the baseline, which is the standard reverse process with $T = 1000$. The HMC sampler adds $L = 2$ extra MCMC steps at each diffusion step t , where each MCMC step constitutes three leapfrog steps. Both sampling methods use the same guidance scale $\lambda = 20.0$. Again, we incorporate the points given by the leapfrog steps, but due to the high dimension, two additional points between each leapfrog step are needed for the line integration. We conduct the same type of parameter search of the step length for the HMC method as in the CIFAR-100 experiment. Further details are provided in appendix A.3.

We sample 50k images with both sampling methods and compute the FID score [11] (based on the validation set), the average accuracy⁴, and the top-5 average accuracy, i.e., correct prediction if the specified label is within the top-5 predictions. Once again, we utilize a separate classifier model, in this case, a RegNetX-8.0GF [26], for evaluation. This time, however, the model is pre-trained. The results are shown in table 3.

The reverse process and HMC perform very similarly in average accuracy, but our method shows a slight improvement in top-5 average accuracy. However, augmenting with some extra MCMC steps with MH-like correction significantly improves the FID score.

⁴Again, an image is considered correctly generated if the classifier’s prediction for the specified class is at least 50%.

Table 3. Average accuracy, top-5 accuracy, and FID score for classifier-full guidance on ImageNet. The metrics are based on 50k generated samples for both sampling methods with score parameterisations. We use the guidance scale $\lambda = 20.0$, $L = 2$ with 3 leapfrog steps for HMC, the step length at diffusion step is $a\beta_t^p$. The accuracy is based on an independent classifier model.

Model	Sampler	Accuracy [%]↑	Top-5 Accuracy [%]↑	FID↓
Score	Reverse	50.0	83.9	14.5
	HMC-6-curve	49.9	85.1	11.6

5.4 Image tapestry

We conduct a so-called image tapestry experiment, similar to the one in [7] and based on their code⁵, as our final experiment. This experiment involves not only the composition of guidance—in this case, classifier-free guidance—but also the composition of combining multiple overlapping text-to-image models. This approach allows us to construct an image with specified content at different spatial locations. Here, we use a pre-trained DeepFloyd-IF⁶ model. For each diffusion step ($T = 100$), 15 extra LA steps were added, with three additional evaluation points for line integration for each step. The guidance scale $\lambda = 20.0$. For more details, see the appendix A.4. In fig. 2a, we can see a generated tapestry image, and in fig. 2b, we can see the specified content at the corresponding spatial locations. There are, in total, nine overlapping content boxes: four are positioned in each corner with different content, while the remaining five are arranged to create a unified image using the same content prompt.

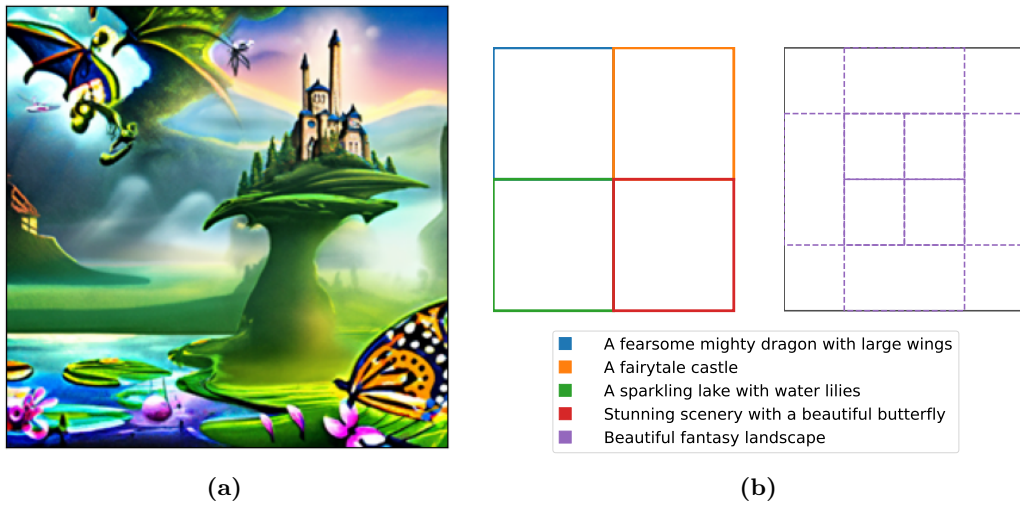


Figure 2. In (a), the generated tapestry image is shown with different content at various spatial locations. In (b), the specified content and their positions are illustrated: on the left, four different contents are displayed in each corner, and on the right, five overlapping content boxes with the same prompt are used to create a unified image.

⁵https://github.com/yilundu/reduce_reuse_recycle

⁶Available at <https://huggingface.co/DeepFloyd/IF-I-XL-v1.0>

6 Discussion

The choice between score and energy parameterisations remains intriguing. We have provided additional empirical evidence that the score parameterisation performs better in the standard reverse process, but that accurate energy estimates can improve more complex sampling methods. We have also demonstrated that most of the gains that may be achieved by using an energy parameterisation can be obtained directly in a score-based model by approximating pseudo-energy differences (probability ratios) using a curve integral of the score function. That is, even though we do not explicitly train an energy-based model, we can perform MH-like correction steps in different MCMC samplers and obtain comparable performance gains.

Particularly interesting is that our trick of using a curve only containing the score evaluations from the standard HMC method seems to perform just as well as the straight line. This means we achieve the correction at practically no extra cost. However, in higher dimensions, additional intermediate steps may be needed, increasing the computational burden. This issue might be mitigated with more efficient integral approximation techniques. Furthermore, it is addressed in latent diffusion, whose primary purpose is to reduce dimensionality. Note, the energy parameterisation always requires an extra differentiation to obtain the score.

The score parameterization is not a proper score function in general, because the vector field it produces is not guaranteed to be conservative. Nevertheless, sampling with the estimated score still performs well in practice. Likewise, using it for the MH-like correction step proposed in our work, seems to achieve significant improvement to the reverse process. However, the invalid assumption of a conservative vector field might explain the small performance edge of the energy parameterisation in the CIFAR-100 experiment, and seeking improved methods for estimating the pseudo-energy difference from a score model is a highly relevant future topic.

7 Conclusion

We have presented a method for extending the reverse diffusion process with MCMC sampling based on an MH-like correction step. Such extended sampling is vital for the composition of pre-trained diffusion models. The MH correction was first presented in [7], where it requires a diffusion model parameterised by an energy function. We propose a method for defining a pseudo-energy difference, which reduces to proper energy differences in the case of a proper score function, and approximating it by numerical integration. This allows us to retain the more common score parameterisation and still perform the MH-like correction. Furthermore, it allows us to use any pre-trained diffusion model in model compositions. MCMC methods that compute internal points, such as HMC, can compute this MH-like correction essentially without any overhead. However, our experiments seem to indicate that the overhead introduced appears to increase with the dimensionality of the diffusion process. We have also presented experiments where the score-parameterised models achieve results comparable to the energy parameterization, indicating that our defined pseudo-energies, although in principle ill-defined, are sufficient to replicate the results from [7] for any diffusion model.

8 Acknowledgments

This work was supported by the Wallenberg AI, Autonomous Systems and Software Program (WASP) funded by the Knut and Alice Wallenberg Foundation. The computations were enabled by resources provided by the National Academic Infrastructure for Supercomputing in Sweden

(NAISS), partially funded by the Swedish Research Council through grant agreement no. 2022-06725.

References

1. Armen Aghajanyan, Lili Yu, Alexis Conneau, Wei-Ning Hsu, Karen Hambardzumyan, Susan Zhang, Stephen Roller, Naman Goyal, Omer Levy, and Luke Zettlemoyer. Scaling laws for generative mixed-modal language models. In *Proceedings of the 40th International Conference on Machine Learning, ICML'23*. JMLR, 2023.
2. Andrew Brock, Jeff Donahue, and Karen Simonyan. Large scale GAN training for high fidelity natural image synthesis. In *International Conference on Learning Representations*, 2019.
3. Tom Brown, Benjamin Mann, Nick Ryder, Melanie Subbiah, Jared D Kaplan, Prafulla Dhariwal, Arvind Neelakantan, Pranav Shyam, Girish Sastry, Amanda Askell, et al. Language models are few-shot learners. *Advances in neural information processing systems*, 33:1877–1901, 2020.
4. Hyungjin Chung, Jeongsol Kim, Michael Thompson Mccann, Marc Louis Klasky, and Jong Chul Ye. Diffusion posterior sampling for general noisy inverse problems. In *The Eleventh International Conference on Learning Representations*, 2023.
5. Jia Deng, Wei Dong, Richard Socher, Li-Jia Li, Kai Li, and Li Fei-Fei. Imagenet: A large-scale hierarchical image database. In *2009 IEEE conference on computer vision and pattern recognition*, pages 248–255. Ieee, 2009.
6. Prafulla Dhariwal and Alexander Nichol. Diffusion models beat GANs on image synthesis. *Advances in neural information processing systems*, 34:8780–8794, 2021.
7. Yilun Du, Conor Durkan, Robin Strudel, Joshua B. Tenenbaum, Sander Dieleman, Rob Fergus, Jascha Sohl-Dickstein, Arnaud Doucet, and Will Sussman Grathwohl. Reduce, Reuse, Recycle: Compositional generation with energy-based diffusion models and MCMC. In Andreas Krause, Emma Brunskill, Kyunghyun Cho, Barbara Engelhardt, Sivan Sabato, and Jonathan Scarlett, editors, *Proceedings of the 40th International Conference on Machine Learning*, volume 202 of *Proceedings of Machine Learning Research*, pages 8489–8510. PMLR, 23–29 Jul 2023.
8. Simon Duane, A.D. Kennedy, Brian J. Pendleton, and Duncan Roweth. Hybrid Monte Carlo. *Physics Letters B*, 195(2):216–222, 1987.
9. Alper Güngör, Salman UH Dar, Şaban Öztürk, Yilmaz Korkmaz, Hasan A Bedel, Gokberk Elmas, Muzaffer Ozbey, and Tolga Çukur. Adaptive diffusion priors for accelerated mri reconstruction. *Medical Image Analysis*, page 102872, 2023.
10. W. K. Hastings. Monte Carlo sampling methods using Markov chains and their applications. *Biometrika*, 57(1):97–109, 1970.
11. Martin Heusel, Hubert Ramsauer, Thomas Unterthiner, Bernhard Nessler, and Sepp Hochreiter. Gans trained by a two time-scale update rule converge to a local nash equilibrium. *Advances in neural information processing systems*, 30, 2017.
12. Geoffrey E Hinton. Training products of experts by minimizing contrastive divergence. *Neural computation*, 14(8):1771–1800, 2002.

13. Jonathan Ho, Ajay Jain, and Pieter Abbeel. Denoising diffusion probabilistic models. *Advances in neural information processing systems*, 33:6840–6851, 2020.
14. Jonathan Ho and Tim Salimans. Classifier-free diffusion guidance. In *NeurIPS 2021 Workshop on Deep Generative Models and Downstream Applications*, 2021.
15. Jonathan Ho, Tim Salimans, Alexey Gritsenko, William Chan, Mohammad Norouzi, and David J Fleet. Video diffusion models. In S. Koyejo, S. Mohamed, A. Agarwal, D. Belgrave, K. Cho, and A. Oh, editors, *Advances in Neural Information Processing Systems*, volume 35, pages 8633–8646. Curran Associates, Inc., 2022.
16. Robert A Jacobs, Michael I Jordan, Steven J Nowlan, and Geoffrey E Hinton. Adaptive mixtures of local experts. *Neural computation*, 3(1):79–87, 1991.
17. Alex Krizhevsky and Geoffrey Hinton. Learning multiple layers of features from tiny images. Technical Report 0, University of Toronto, Toronto, Ontario, 2009.
18. Yann LeCun, Sumit Chopra, Raia Hadsell, M Ranzato, Fugie Huang, et al. A tutorial on energy-based learning. *Predicting structured data*, 1(0), 2006.
19. Yujia Li, David Choi, Junyoung Chung, Nate Kushman, Julian Schrittwieser, Rémi Leblond, Tom Eccles, James Keeling, Felix Gimeno, Agustin Dal Lago, et al. Competition-level code generation with alphacode. *Science*, 378(6624):1092–1097, 2022.
20. Nan Liu, Shuang Li, Yilun Du, Antonio Torralba, and Joshua B Tenenbaum. Compositional visual generation with composable diffusion models. In *European Conference on Computer Vision*, pages 423–439. Springer, 2022.
21. David Lüdke, Marin Biloš, Oleksandr Shchur, Marten Lienen, and Stephan Günnemann. Add and thin: Diffusion for temporal point processes. In *Thirty-seventh Conference on Neural Information Processing Systems*, 2023.
22. Guy Mayraz and Geoffrey E Hinton. Recognizing hand-written digits using hierarchical products of experts. *Advances in neural information processing systems*, 13, 2000.
23. Nicholas Metropolis, Arianna W. Rosenbluth, Marshall N. Rosenbluth, and Augusta H. Teller. Equation of state calculations by fast computing machines. *The Journal of Chemical Physics*, 21(6):1087–1092, 1953.
24. Radford M. Neal, P. Diggle, and S. Fienberg. *Bayesian Learning for Neural Networks*. Lecture Notes in Statistics Ser.: v.118. Springer New York, 1996.
25. Alexander Quinn Nichol and Prafulla Dhariwal. Improved denoising diffusion probabilistic models. In *International Conference on Machine Learning*, pages 8162–8171. PMLR, 2021.
26. Ilija Radosavovic, Raj Prateek Kosaraju, Ross Girshick, Kaiming He, and Piotr Dollár. Designing network design spaces. In *Proceedings of the IEEE/CVF conference on computer vision and pattern recognition*, pages 10428–10436, 2020.
27. G. O. Roberts and O. Stramer. Langevin diffusions and Metropolis–Hastings algorithms. *Methodology & Computing in Applied Probability*, 4(4):337 – 357, 2002.
28. Chitwan Saharia, William Chan, Saurabh Saxena, Lala Li, Jay Whang, Emily L Denton, Kamyar Ghasemipour, Raphael Gontijo Lopes, Burcu Karagol Ayan, Tim Salimans, et al. Photorealistic text-to-image diffusion models with deep language understanding. *Advances in Neural Information Processing Systems*, 35:36479–36494, 2022.

29. Tim Salimans and Jonathan Ho. Should EBMs model the energy or the score? In *Energy Based Models Workshop - ICLR 2021*, 2021.
30. Karen Simonyan and Andrew Zisserman. Very deep convolutional networks for large-scale image recognition. *arXiv preprint arXiv:1409.1556*, 2014.
31. Jascha Sohl-Dickstein, Eric Weiss, Niru Maheswaranathan, and Surya Ganguli. Deep unsupervised learning using nonequilibrium thermodynamics. In *International conference on machine learning*, pages 2256–2265. PMLR, 2015.
32. Jiaming Song, Arash Vahdat, Morteza Mardani, and Jan Kautz. Pseudoinverse-guided diffusion models for inverse problems. In *International Conference on Learning Representations (ICLR)*, May 2023.
33. Yang Song and Stefano Ermon. Generative modeling by estimating gradients of the data distribution. *Advances in neural information processing systems*, 32, 2019.
34. Yang Song, Jascha Sohl-Dickstein, Diederik P Kingma, Abhishek Kumar, Stefano Ermon, and Ben Poole. Score-based generative modeling through stochastic differential equations. In *International Conference on Learning Representations*, 2021.
35. Cédric Villani. *The Wasserstein distances*, pages 93–111. Springer Berlin Heidelberg, Berlin, Heidelberg, 2009.
36. Kai Wang, Zhaopan Xu, Yukun Zhou, Zelin Zang, Trevor Darrell, Zhuang Liu, and Yang You. Neural network diffusion, 2024.
37. Jamie Wynn and Daniyar Turmukhambetov. DiffusioNeRF: Regularizing neural radiance fields with denoising diffusion models. In *Proceedings of the IEEE/CVF Conference on Computer Vision and Pattern Recognition*, pages 4180–4189, 2023.

A Experimental details

Here we provide more details about the four different conducted experiments: 2D composition, guided diffusion for CIFAR-100, guided diffusion for ImageNet, and Image tapestry.

A.1 2D composition

The composed distribution is defined by a product of two components, a Gaussian mixture and a uniform distribution with non-zero values on

$$\square = \{x \in \mathbb{R}^2 : -s_i \leq x_i \leq s_i, i = 1, 2\}, \quad (22)$$

where s_1 and s_2 are equal to 0.2 and 1.0, respectively. The eight modes of the Gaussian mixture are evenly distributed on a circle with a radius of 0.5 at the angles $\frac{\pi}{4}i$ for $i = 0, \dots, 7$, respectively. The covariance matrix at each mode is $0.03^2 \cdot I$, where I is the identity matrix.

The metric log-likelihood is ill-defined as we may generate samples where the true distribution has no support (due to the uniform distribution). We address this problem by expanding the definition set of the uniform distribution and redistributing one percent of the probability mass into this extended region. The whole set is defined as (22) except $s_1 = s_2 = 1.1$. Note that 99 percent probability mass remains inside the original definition set \square .

We use the same neural network architectures as the base for both the score and energy models. It is a residual network consisting of a linear layer (dim $2 \rightarrow 128$) followed by four blocks, and concluding with a linear layer (dim $128 \rightarrow 2$). Within each block, the input x passes through a normalization layer, a SiLU activation, and a linear layer (dim $128 \rightarrow 256$). Subsequently, it is added with an embedded t (dim 32) that has undergone a linear layer transformation (dim $32 \rightarrow 256$). The resulting sum passes through a SiLU activation and is further processed by a linear layer (dim $256 \rightarrow 256$). After that, another SiLU activation is applied, followed by a final linear layer (dim $256 \rightarrow 128$). The output of this linear layer is then added to the original input x within the block. The embedding of t is also learnable.

The parameter β_t follows the cosine schedule proposed in [25]. For (U-)HMC, the damping coefficient is set to 0.5, the mass diagonal matrix has all diagonal elements equal to 1, and the stepsize for each t is 0.03. For (U-)LA, the stepsize for each t is set to 0.001.

A.2 Guided diffusion for CIFAR-100

The parameter β_t has a linear schedule as originally proposed in [13]. For (U-)HMC is the damping coefficient equal to 0.9 and the diagonal elements in the massmatrix are equal to β_t for each t . The values of the stepsize parameters a and b were determined through a simple parameter search for the different MCMC methods and they can be found in table 4. This was done for both the score and energy parameterizations, where the stepsize is defined as $\delta_t = a\beta_t^b$.

A.3 Guided diffusion for ImageNet

Again, the parameter β_t follows a linear schedule. The hyperparameters for the HMC include a damping coefficient set at 0.9, with the diagonal elements of the mass matrix being equal to β_t for each t . The stepsize parameters for HMC, obtained from a simple parameter search, are $a = 1.87$ and $b = 1.51$.

Table 4. The values of the stepsize parameters a and b obtained from a random parameter search for the different MCMC methods for both score and energy parameterization in the CIFAR-100 experiment, where the stepsize is defined as $\delta_t = a\beta_t^b$.

Model	MCMC	Stepsize Parameters	
		a	b
Energy	U-LA	9.22	1.40
	LA	9.84	0.83
	U-HMC	0.26	1.53
	HMC	9.33	1.48
Score	U-LA	1.96	1.04
	LA	9.84	0.83
	U-HMC	0.26	1.53
	HMC	4.03	1.34

A.4 Image tapestry

A cosine schedule is used for the parameter β_t . The stepsize parameters in this case is simply $a = 1$ and $b = 1$, i.e., $\delta_t = \beta_t$.